WILEY-VCH

DOI: 10.1002/((please add manuscript number))
Article type: Full paper

Multi-Effects Coupled Nanogenerators for Simultaneously Harvesting Solar, Thermal and Mechanical Energies

*Wenxuan Zhu, Chaosheng Hu, Maoyi Zhang, Tao Jiang, Chris R. Bowen, Xiaojing Mu, Ya Yang**

W. Zhu, Prof. T. Jiang, Prof. Y. Yang, School of Chemistry and Chemical Engineering, Center on Nanoenergy Research, Guangxi University, Nanning, Guangxi, 530004, PR China.
W. Zhu, C. Hu, M. Zhang, Prof. T. Jiang, Prof. Y. Yang, CAS Center for Excellence in Nanoscience, Beijing Key Laboratory of Micro-nano Energy and Sensor, Beijing Institute of Nanoenergy and Nanosystems, Chinese Academy of Sciences, Beijing 101400, P. R. China.
Corresponding author. E-mail: yayang@binn.cas.cn
C. R. Bowen, Department of Mechanical Engineering, University of Bath, BA27AK, UK.
Prof. X. Mu, Defense Key Disciplines Lab of Novel Micro-nano Devices and System Technology, Chongqing University, Chongqing 400044, China.
Prof. Y. Yang, School of Nanoscience and Technology, University of Chinese Academy of Sciences, Beijing, 100049, China.

Keywords: Coupled nanogenerators, energy harvesting, coupling factor, BNT.

1. Introduction

With the increasing growth and technological developments in our society, the demand for energy at large and small-scale continues to grow. With respect to sustainable development and environmental considerations, efforts to make better use of green energy such as light, heat, and wind has therefore become research topic of significant interest. [1-4] There are a wide variety of ambient forms of energy in our daily environment [5-8], and these dispersed energy forms often cannot be readily

collected by an individual device at a large scale. For this reason, small-scale energy harvesting and conversion devices have received increasing attention, such as the photovoltaic cell (PVC) [9,10], piezoelectric nanogenerator (PiENG) [11,12], pyroelectric nanogenerator (PyENG) [13,14], and triboelectric nanogenerator (TENG) [1,15]. Nevertheless, since our ambient environment is often complex and changeable, multiple types of energy often exist simultaneously, and the simultaneous collection of multiple forms of energy to generate electrical energy is an important consideration [16,17].

Recently, there has been a number of reports on multi-functional composite nanogenerators and coupled nanogenerators [3,14,17,18], where researchers have considered combinations of energy harvesters that are able to harvest different forms ambient energy; these have included (i) a combined electromagnetic generator (EMG) and TENG [19,20], (ii) a combined PiENG and TENG [6,11], (iii) a combined PVC and PyENG [21,22] and (iv) a combined TENG-PiENG-EMG[23,24]. Since these devices often use individual external circuits and connections, they often exhibit a complex device structure. Therefore, a coupled nanogenerator with single-structure and single pair of output electrodes has been investigated [17,18,25]. This approach solves the complex structural problem, while also enabling interactions between the individual reactions, which facilitates the output performance. This design is usually based on materials with multifunctional electrical properties, such as ferroelectric materials [9,26,27], which can exhibit photoelectric, pyroelectric, and piezoelectric properties at the same time [21,28-30]. However, when these various mechanisms are combined, they

often do not always operate cooperatively and interact intermittently with each other constructively or destructively, thereby reducing the harvested output [3,31,32]. There are therefore challenges to be solved for coupled nanogenerators based on ferroelectric materials, including new device structures and new methods to evaluate the performance enhancement when there is constructive coupling and the evaluation of the degree of coupling in the range of available ferroelectric materials [2,25,27,33].

In this paper, we therefore have developed a novel single-structure and multi-harvesting coupled nanogenerator [14,17,25] based on the unique photoelectric, pyroelectric and piezoelectric properties of BNT ceramics [4,9], which is exploited to collect light, heat and mechanical energy simultaneously. In order to demonstrate the enhanced performance of this coupled nanogenerator, we compare in detail the harvesting performance of the nanogenerator with each harvesting mechanism operating independently (uncoupled), with the performance when harvesting mechanisms are operating simultaneously (coupled); where the coupled performance is shown to be enhanced. In addition, we have defined a new harvesting coupling factor to evaluate the degree of coupling to compare the coupling performance of different materials. Our comparison shows that the coupling enhancement of BNT is the best under heating condition, while the coupling enhancement effect of PZT is the best under cooling conditions. This study therefore provides a new device design and a new evaluation basis for the further development of coupled nanogenerators with multiple harvesting effects, and can inform the future enhancement of the performance of coupled nanogenerators.

2. Results and Discussion

Harvester structural design. As a ferroelectric material, BNT has a variety of important dielectric properties to design a multi-effect coupled nanogenerator. The design principle is shown in **Figure 1a**, where the multi-effect coupled nanogenerator combines a photovoltaic cell (PVC) to harvest light, a pyroelectric nanogenerator (PyENG/PENG) to harvest thermal energy, and a triboelectric-piezoelectric nanogenerator (TPiENG) to harvest mechanical energy. This approach combines multiple harvesting mechanisms that interact cooperatively to improve output performance. The coupled nanogenerator exhibits a multi-layer structure, with a specific structure as shown in **Figure 1b**, where the left image is the overall structure diagram, and the right frame is a partially enlarged image. As can be seen, from the bottom to the top, the first approach is to achieve heating and cooling of a thermoelectric (TE) module to ensure that good heat dissipation of the metal heat sink in achieved during testing. The BNT ceramic has an upper indium tin oxide (ITO) electrode and an Ag electrode is sputtered on each of its upper and lower surfaces. The transparent ITO electrode is used as the upper electrode to allow light harvesting, the Ag electrode as the bottom electrode, and the BNT ceramic is used as a photoelectric, pyroelectric and piezoelectric material. Nylon films are attatched on the ITO electrodes, and fluorinated ethylene propylene (FEP) films are fixed with acrylic plates, where both contact-separation occurs during motion to act as a single-electrode triboelectric nanogenerator. In addition, the FEP film provides external strain to the BNT ceramic to form a piezoelectric nanogenerator (PiENG). The coupled

nanogenerator of this structure has a simple structure and only has a single pair of electrodes, which can collect various forms of energy and convert them into electrical energy. Its physical map can be seen in **Figure 1c**, and the structure of each layer of the coupled nanogenerator can be observed. The diameter of the BNT ceramic in this device is 1.6 cm, as seen in **Figure 1d**, with a scale of 1 cm.

Individual harvesting (uncoupled) performance. The harvesting performance of each component of the coupled nanogenerator when operating independently is initially evaluate, as shown in **Figure 2**. For the photovoltaic cell (PVC) element, testing was conducted during illumination by an LED light source, and the output current and output voltage are shown in **Figure 2a** and **Figure 2b** respectively, where the wavelength of the LED light source is 405 nm and the light intensity is 180 mW/cm^2. In **Figure 2a**, when the device is illuminated, a ~ 200 nA spike is generated due to a combination of the photovoltaic effect and the pyroelectric effect, due to a temperature change induced by the light; when the light-induced temperature change is constant, only the net photovoltaic effect remains, and the current exhibits a stable plateau of 78 nA. As shown in **Figure 2b**, due to the influence of the parallel resistance, the output voltage does not exhibit spikes, and the plateau voltage is 11 V. **Figure 2c** shows the output platform current and corresponding instantaneous power with different external load resistances. It can be seen that when the external resistance is 300 MΩ, which represents the matched impedance between the harvesting device and electrical load, where the maximum power is 0.27 μW.

When the pyroelectric nanogenerator (PyENG) is operating independently, the temperature change is controlled by a cooling sheet to test its output in the absence of light. A cyclic temperature difference of ΔT ~ 35.5K is applied, where the temperature-time profile is shown in Figure S1. When the temperature rises, a sharp pyroelectric signal is generated due to the decrease in the polarization of the ferroelectric. When the temperature remains unchanged, the pyroelectric signal falls to zero since there is no change in polarization. When the temperature falls and recovers, an equivalent magnitude pyroelectric signal is generated as a reverse electrical signal, since there is now an increase in the polarisation level. The output current in this case is shown in **Figure 2d** with a peak current of 240 nA; the output voltage is shown in **Figure 2e** with a peak voltage of 30 V. **Figure 2f** shows the peak current and corresponding instantaneous power of the pyroelectric nanogenerator when different load resistances are applied. When the applied resistance is 300 MΩ the maximum power is 5.32 μW, representing condition of impedance matching between the load and device, which is consistent with the photovoltaic cell element.

To evaluate the triboelectric-piezoelectric nanogenerator (TPiENG) operating independently, a test was carried out when mechanical energy is applied in the form of wind at a speed of 10m/s. During flutter of the FEP film in the wind, the triboelectric signal can be seen in **Figure 2g** and **Figure 2h**, where the average value of the maximum output current is 1.3 μA. The voltage produced is a result of the cancellation of charge between the triboelectric effect and the piezoelectric effect, where the baseline swings and the signal are small, less than 1 V. **Figure 2i** shows the

current and corresponding instantaneous power of TPiENG when different load resistances are applied, and the maximum power is 0.2 μW when the load resistance is impedance matched to the device as is 400 kΩ.

The test conditions for each element are varied and the performance of each harvesting mechanism is further investigated. For the photovoltaic cell, the intensity of the LED light source on the BNT ceramic was changed for testing, which the output current for a range of light intensities is shown in **Figure 3a**, and the output voltage is shown in **Figure 3b**. As the light exposure level rises, the output current, the peak current, the plateau current and the output voltage increases. For the pyroelectric nanogenerator component, tests were performed under a range of cooling ($\Delta T < 0$) and heating ($\Delta T > 0$) conditions. As a result of the change in surface temperature of the BNT with time (**Figure 3c**), the pyroelectric current-time is shown in **Figure 3d**, and the pyroelectric voltage signals curve is shown in **Figure 3e**. Under conditions of cooling, negative current and voltage signals are generated, while under conditions of heating, positive current and voltage signals are produced. The limitation of heat dissipation conditions leads to unstable current under a large temperature difference maintained during heating, while the change in positive voltage output that should be generated when cooling is stopped under a large temperature difference condition is not obvious. The peak pyroelectric current and pyroelectric voltage with temperature difference are summarized, and the current and voltage versus temperature difference curve is obtained as shown in **Figure 3f**. It can be seen that a linear relationship is observed as the temperature difference (ΔT) varied

from -17.4 K to 29.8 K, the peak current varied from -0.201 μA to 0.261 μA and the peak voltage varied from -23.582 V to 31.449 V. The pyroelectric response is relflected by pyroelectric coefficient (P_c) [13,34], namely:

$$P_c = Q / (S\Delta T) \quad (1)$$

Where, Q is the net charge caused by temperature change (ΔT) in one cycle, which was obtained by integrating the pyroelectric current with time, and S is the effective electrode area (2.01 cm^2). **Figure 3g** shows the relationship between the surface charge density (Q/S), P_c and the temperature change (ΔT). The surface charge density is positively correlated with the absolute value of the temperature difference (ΔT), and the pyroelectric coefficient is relatively stable, remaining in the range of P_c ~ 43.6 - 52.4 nC cm^{-2} K^{-1}. For the triboelectric-piezoelectric component (TPiENG), the current signals at different wind speeds can be obtained, as shown in Figure S2a; if the Nylon film in **Figure 1b** is replaced with a FEP film, no friction signal will be generated during the collecting of wind energy, and the current of PiENG under different wind speeds can be obtained. The signal, shown in Figure S2b, is approximately half of the current signal in the presence of TPiENG.

Coupled output performance. We now characterize the device when subjected to more than one energy source. This is achieved by coupling the individual harvesting components in the multi-effect coupled nanogenerator in pairs (e.g. light and heat), and we characterize the device when two of the three kinds of energy, namely light, heat and mechanical movement occur simultaneously. The coupling effect of a combined PVC and TPiENG is measured by providing both illumination and wind

simultaneously by a light source and a fan. When illuminated by a 405 nm LED light source with an intensity of 180 mW/cm^2, and a changing wind speed, the current-time curves of the coupled TPiENG and PVC are compared with single PVC and TPiENG units operating independent (uncoupled) for different wind speeds, as shown in Figure S3. Because there are multiple variables in the testing process, the wind speed condition of 10 m/s is chosen for the two conditions of light and wind, considering the difference in magnitude of the two signals and the error caused by the measuring instrument. When the wind speed is 10 m/s, the current-time curve is shown in **Figure 4a**, where it can be observed that the coupled current increases in the positive direction and decreases in the negative direction compared with TPiENG, which is equivalent to shifting the baseline of TPiENG upward to the platform current of the PVC.

The coupling effect between PVC and PyENG was measured by cooling and heating the materials when subjected to illumination. Under the application of light at a constant intensity and changing the temperature, a comparison of the current-time curves under combined cooling and lighting conditions with that of cooling alone (Figure S4) and the comparison of the current-time curves under combined heating and lighting conditions with that under heating alone (Figure S5) can be obtained. **Figure 4b** shows the current generated when light is applied during cooling, with a cyclic temperature difference of ΔT = -22 K. Since the pyroelectric signal generated during cooling is opposite in sign compared to the photovoltaic signal, there is difference in the current response with time. A positive peak signal of 233.6 nA was

observed on heating and cooling yielded a negative peak signal of -55.3 nA, with a plateau current of 47.5 nA. **Figure 4c** shows the current generated by simultaneous illumination and heating with a temperature difference of ΔT = 32.9 K, with a large positive peak signal of 315.9 nA generated by the positive coupling of photovoltaic and pyroelectric effects, with a plateau current of 149.2 nA, which is larger than that of the PyENG and PVC operating independently (uncoupled). On summarizing the platform currents for a range of temperature differences, **Figure 4d** can be obtained, where it can be seen that the platform current of a single PyENG is close to 0, and the platform current on coupling light and cooling is smaller than that of a single PVC since the currents are opposite in sign. However, on coupling light and heating the output is larger than a single PVC since the generated currents operate constructively and a positive coupling effect can be observed. The current-time curves within 60 s of each thermal cycle are then integrated to obtain the transferred charge on coupling the PVC and PyENG and compared with the individual transferred charges of each component, as shown in **Figure 4e**. The transferred charges generated by the individual PVC in each test are similar, with an average value of 5.07 μC, while the transferred charges of the individual PyENG component increased with an increase in temperature difference. It can be observed that the transferred charge when coupled is improved during cooling for the PyENG, but attenuates for the PVC. However, during heating, the transferred charge on coupling is greatly improved. When the temperature increase is ΔT = 32.9 K, the transferred charge after coupling is 10.48 μC, which is

larger than the sum of the individual components; namely 2.08 μC for the PyENG and 5.07 μC for the PVC.

For the combined TPiENG and PyENG, subjected to a fixed wind speed of 10 m/s, cooling or heating can be applied, and a comparison of the current-time response under different temperature differences of each individual component can be obtained; different cooling conditions can be seen in Figure S6, and different heating conditions can be seen in Figure S7. When the temperature difference is ΔT = -25.1 K during cooling, the current-time curve shown in **Figure 4f** is obtained, and a negative peak corresponding to the PyENG is generated when coupled; the pyroelectric current is typically smaller than the current generated by the TPiENG. During heating, when the temperature difference is ΔT = 44.1 K, it can be seen in **Figure 4g** that a positive peak corresponding to PyENG is generated during coupling, and the maximum can reach 1.3 μA.

When the various effects of light, heat and wind act on the multi-effect coupled nanogenerator simultaneously, the enhanced performance of the coupled nanogenerator can be demonstrated by comparing the individual components. During the experiment, we found that for BNT, the polarization direction will be opposite when the direction of the applied electric field is opposite, then the positive and negative poles of BNT will change. So, the change of polarization direction will change the direction of the pyroelectric current and photovoltaic current, but since their current directions change in the same direction, then it will not affect the output magnitude of coupled nanogenerators. When the wind speed is 10 m/s and the light

intensity is 180 mW/cm^2, heating is applied, and when the temperature difference is ΔT = 35 K, the current of the individual components and the current under all combined conditions are evaluated, as shown in **Figure 5a**. The charge transfer curve can also be obtained by integrating the current in each cycle for 60 s. The transfer charge of the photovoltaic cell when acting independently is 4.677 μC, the transfer charge of the pyroelectric generator acting independently is 2.838 μC, and the transfer charge of the triboelectric-piezoelectric component acting independently is 0.119 μC. However, the transferred charge after coupling the three elements is 9.849 μC, which is greater than the sum of the individual component and has a significant effect of the degree of coupling. In addition, a comparison of the voltage signals curves of the separate components (uncoupled) and when coupled can be seen in Figure S8. The voltage peak after the coupling falls since the application ofwind leads to increased dissipation of heat for the same heating conditions, and the temperature has decreased compared with that of the single component. In the case of applying different external load resistances, the instantaneous current for coupled conditions can be measured, and the corresponding power is obtained; the current-power curve can be seen in Figure S9. On comparing the power curve obtained by each individual component (uncoupled) with that after coupling, as shown in **Figure 5c**, the power after coupling is 7.73 μW, which is greater than operating individually, and the optimal matching resistance is 100 MΩ. As shown in **Figure 5b**, by integrating the current curve under the optimal impedance conditions, the maximum harvested energy of the single components and the coupled device can be obtained, where the photovoltaic cell is

15.30 μJ, the pyroelectric generator is 56.60 μJ, the triboelectric-piezoelectric component is 3.02 μJ, and the coupled system is 67.78 μJ. For a better practical evaluation of the output performance, a 1 μF capacitor was charged after attaching each individual element and the coupled nanogenerator through a rectifier bridge. For the same harvesting time of 300 s, a charging curve is shown in **Figure 5d**, where the coupled nanogenerator can increase the voltage across the capacitor to 29 V, while the single photovoltaic cell is 12 V, the single pyroelectric is 18 V, and the TPiENG component is 22V. The specific output current and voltage after rectification of each part can be seen in Figure S10. In order to more intuitively reflect the improved performance of the multi-effect coupled nanogenerator, data are summarized on a radar chart and compared with the performance of each part acting independently. As shown in **Figure 5e**, the current magnitude, transferred charge, instantaneous power, maximum energy, maximum voltage and voltage across the capacitor are compared respectively. The specific data can be seen in the previous discussion. It can be seen from the figure that the coupled nanogenerator has a performance area is much larger than the individual sections. The stability of the nanogenerators in the paper was demonstrated by using the same set-up throughout the experiments, and various repeated tests maintained the consistency of the signals. On the working mechanism of coupled nanogenerators, the polarized BNT devices lead to carrier separation and transport due to the polarization electric field and the built-in electric field. Under the illumination condition, the photogenerated electron holes are divided into positive and negative charges to form photovoltaic currents, while pyroelectric currents are

generated due to the photothermal effect. Under the simultaneous effect of light and heating, the mobility of photogenerated carriers is increased, generating larger photocurrents. And under wind-blown conditions, the BNT ceramic generates piezoelectric signals due to the piezoelectric effect, while the charge on the surface of the ITO electrode is transferred due to the contact separation of the triboelectric materials and electrostatic induction, which generates triboelectric signals.

Since the coupling enhancement refers to the increase of generated charge, a *Yang coupling factor* ($k_{C,Q}$) can be defined as the sum of the charge after coupling, divided by the charge of each individual component, as follows:

$$k_{C,Q} = q / \Sigma q_i \qquad (2)$$

Here, q is the transferred charge after coupling and q_i (i=1, 2, 3, …) is the transferred charge for each individual component. By calculating the coupling factor, the performance of a range of ferroelectric materials in coupled nanogenerators can be evaluated and compared. A coupling factor $k_{C,Q} > 1$ indicates a constructive combination of charge during a harvesting cycle, while a $k_{C,Q} < 1$ indicates a destructive combination of charge. Common ferroelectric materials BNT, lead zirconate titanate (PZT), barium titanate (BTO) and polyvinylidene difluoride (PVDF) are tested under the same conditions, and the current curves and corresponding charges of the individual parts and after coupling can be obtained. For the comparison of ferroelectric properties, we measured the ferroelectric hysteresis loop of BNT, BTO and PZT (see Figure S11 in the supporting information) and the d_{33} constant after polarization. It can be seen from the figure that has ferroelectric properties. In

addition, the d_{33} constant of PZT is 500, the d_{33} constant of BTO is 150, and the d_{33} constant of BNT is 80. For example, Figure S12 shows the coupling of BNT under cooling conditions; Figure S13-15 show the coupling of PVDF, PZT and BTO under heating and cooling conditions, respectively. By calculating the coupling factor for comparison, a comparison graph can be obtained as shown in **Figure 5f**, from which it can be seen that the coupling factor $k_{C,Q}$ of BNT is 1.29 during heating, which is the largest compared with other materials, proving that the coupled nanogenerator with multiple effects prepared using BNT has the best performance when heated. While the coupling factor of PZT is 1.26 under cooling conditions, which is the best coupling effect during cooling. These differences during heating and cooling are a result of the different photovoltaic, pyroelectric and piezoelectric properties of the ferroelectric materials.

Coupled nanogenerators can be mainly applied in places where wind energy is abundant, light resources are abundant, and the temperature difference between day and night is large. For example, they can be applied to wind power plants, which can collect not only the wind energy that exists all year round, but also the light and heat energy during the day, and these energies can be stored through capacitors and supply power to various temperature and wind speed sensors in wind power plants. The same application scenarios are also on both sides of the highway, the sea lighthouse, etc.

3. Conclusion

In conclusion, this paper demonstrates a novel coupled nanogenerator device that is capable of exploiting the unique photoelectric, pyroelectric and piezoelectric

properties BNT ceramics to realize energy harvesting of multiple energy source. The improved harvesting performance of the BNT coupled nanogenerator was observed by assessing the harvesting performance of each component of the nanogenerator independently (uncoupled), two-by-two coupling (e.g. light and heat) and multiple coupling (light, heat and mechanical). The harvested current magnitude, transferred charge, instantaneous power, maximum energy, maximum voltage, and voltage across the capacitor were compared. In contrast to previous studies, this paper evaluates in detail the degree of enhancement of coupled nanogenerators in terms of improved output performance [14,17], which is clearly reflected by radar plots in **Figure 5e**. In addition, to evaluate the degree of coupling, a new coupling factor ($k_{C,Q}$) was defined from the perspective of transferred charge, and the magnitude of the coupling factor can be used to determine the degree of coupling under a range of harvesting conditions. Several ferroelectric materials were evaluated, and the magnitude of the coupling factor indicated that BNT has the best coupling enhancement during heating. The definition of a new form of coupling factor from the perspective of transferred charge, allows us to quantitatively analyze the degree of coupling and enhancement when harvesting multiple forms of ambient energy.

This paper therefore provides new directions for the development of coupled nanogenerators with multiple harvesting mechanisms, bringing together a photovoltaic cell, pyroelectric nanogenerator and triboelectric-piezoelectric nanogenerator into a unique single structure to operate cooperatively. This has contributed to the development of coupled nanogenerators that harvest various types

of energy from the environment and has great promise for application in the field of self-powered electronic devices.

4. Experimental Section

Raw materials. Bismuth oxide (Bi_2O_3), titanium dioxide (TiO_2) and sodium carbonate (Na_2CO_3) were used as raw materials for the preparation of $Bi_{0.5}Na_{0.5}TiO_3$ (BNT), and were purchased in analytically pure form from Shanghai Maclin Biochemical Technology Company Limited. Barium titanate (BTO) was purchased from Shanghai Aladdin Biochemical Technology Company Limited, and its specifications were analytically pure. The polyvinyl alcohol (PVA) was obtained from Beijing Yili Fine Chemicals Company Limited, the PZT was obtained from Quanzhou Phi Phi Trading Company Limited, and the PVDF was obtained from Jinzhou Kexin Electronic Materials Company Limited.

Preparation of $Bi_{0.5}Na_{0.5}TiO_3$ (BNT) ceramics. First, a specific mass of Na_2CO_3, Bi_2O_3, and TiO_2 raw materials were placed in a vacuum drying oven and dried at 120 °C. Then, they were weighed according to its stoichiometric ratio, placed into a ball mill jar and mixed, and a suitable amount of anhydrous ethanol was added. The ball mill was used for 12 h to ensure they were fully mixed. After that, the mixed material was removed and placed into a vacuum drying oven for drying at 120 °C to obtain a well-mixed powder. The obtained powder was pressed into a column, and the column was placed in a muffle furnace and calcined at 850 °C for 1 h to obtain the product. After grinding and crushing the calcined column, it was reintroduced into the

ball mill jar and ball milled for 12 h and dried to obtain the BNT powder. The BNT powder was then mixed with a few drops of PVA and ground well for pressing, then placed into a muffle furnace, firstly it was heated to 650 ℃ for one hour to remove the PVA, then sintered at 1150 ℃ for 2 h the form the BNT ceramics. After sintering, sandpaper was used to polish the ceramic to obtain a thickness of approximately 200 μm, and after cleaning the surface, the top and bottom surfaces were sputtered with silver Ag and indium tin oxide (ITO) as test electrodes. Finally, the electrode ceramics were placed into silicone oil and polarized at 800 V for 30 min.

Characterization and measurements. Firstly, the BTO powder was mixed with a several drops of PVA and ground sufficiently for pressing, and then placed into a muffle furnace. The temperature raised to 650 °C for one hour to remove the PVA, and then held at 1200 °C for 2 h to sinter and form the BTO ceramics. Sandpaper was used to polish the ceramics to obtain a thickness of approximately 200 μm, and after cleaning the surface, the upper and lower surfaces are sputtered with silver Ag and indium tin oxide (ITO) as test electrodes. Finally, the samples were placed into silicone oil and polarized at 600 V for 30 min.

Fabrication of coupled nanogenerators. A semiconductor cooler was fixed on a metal heat sink using thermal conductive adhesive, where a layer of aluminum tape was applied on the semiconductor cooler to form the base electrode, and silver paste was used to connect the aluminum tape to the Ag electrode of the ITO/BNT/Ag ceramic. Then, a wire was applied on the top ITO electrode with silver paste and a wire was applied to aluminum tape. The top of the ITO/BNT/Ag ceramic was then

covered with a layer of nylon film as a friction material, and the other friction material was FEP film (160×12×0.06 mm^3). A laser cutter (PLS4.75, General Laser Systems, USA) was used to cut the acrylic plate as the support layer extending from left to right at the bottom and the support layer at the top, which was fixed using the acrylic plate and screw nuts at a distance of 3 mm from the nylon film. The area of the BNT ceramic disk was approximately 2.01 cm^2. The fabrication process of the coupled nanogenerators based on other ferroelectric materials was the same as above, only the ceramic was changed.

Characterization and measurements. The piezoelectric coefficients of the materials were tested using a quasi-static piezoelectric constant d_{33} tester (ZJ-4AN, Institute of Acoustics, Chinese Academy of Sciences). The light density on the device surface was measured by a laser power meter (PD300, OPHIR, Israel) with a 405 nm LED (Beijing Jolyhan Light Instruments Co., Ltd.) as the light source, and different light intensities could be achieved by filtering the filter or adjusting the distance. A semiconductor cooling chip (XH-C1206, Jiangsu Xinghe Electronic Technology Co., Ltd.) was used to provide the temperature change, and the temperature could be regulated by a programmable DC power supply (KEITHLEY 2260B, Tektronix, USA) with different applied voltage. The temperature changes of the device surface were detected and recorded by an infrared thermography pyrometer (PI400O38T900, Optris, Germany). Current and voltage signals were tested using a digital source meter (KEITHLEY 2611B, Tektronix, USA). In this paper, the ferroelectric properties of

ferroelectric ceramics were tested by a ferroelectric test system (Radiant Precision Multiferroic II).

Supporting Information

Supporting Information is available online from the Wiley InterScience or from the author.

Acknowledgements

This work was supported by the National Key R & D Project from Minister of Science and Technology in China (No. 2021YFA1201604), the National Natural Science Foundation of China (No. 52072041), the Beijing Natural Science Foundation (Grant No. JQ21007), the Beijing Nova Program (Grant No. Z211100002121086) and the University of Chinese Academy of Sciences (Grant No. Y8540XX2D2). The authors also gratefully acknowledge financial support from project of open foundation from Defence Key Disciplines Lab of Novel Micro-Nano Devices and System Technology graduate scientific research and innovation foundation of College of Optoelectronic Engineering, Chongqing University, Chongqing, China (Grant No. GDYKC202004).

Author contributions: Y.Y. conceived the idea and supervised the research. W.Z., C.H. and M.Z. fabricated the composite materials, carried out the device fabrication and the performance measurement. W.Z, C.R.B., T.J., X.M. and Y.Y. analyzed the data and cowrote the manuscript. All authors read and revised the manuscript.

Received: ((will be filled in by the editorial staff))
Revised: ((will be filled in by the editorial staff))
Published online: ((will be filled in by the editorial staff))

[1] Q. Bai, X.W. Liao, Z.W. Chen, C.Z. Gan, H.X. Zou, K.X. Wei, Z. Gu and X.J. Zheng, *Nano Energy* **2022**, *96*.

[2] X. Chen, Y. Zhao, F. Wang, D. Tong, L. Gao, D. Li, L. Wu, X. Mu and Y. Yang, *Adv. Sci. (Weinh)* **2022**, *9*, e2103957.

[3] H. Cho, S. Jo, I. Kim and D. Kim, ACS *Appl. Mater. Interfaces* **2021**, *13*, 48281-48291.

[4] P. Li, J. Zhai, H. Zeng, B. Shen, W. Li and K. Zhao, *J. Eur. Ceramic Soc.* **2016**, *36*, 3139-3145.

[5] U. Khan and S. W. Kim, *ACS Nano* **2016**, *10*, 6429-6432.

[6] E. J. Lee, T. Y. Kim, S.W. Kim, S. Jeong, Y. Choi and S. Y. Lee, *Energy Environ. Sci.* **2018**, *11*, 1425-1430.

[7] J. Wang, W. Ding, L. Pan, C. Wu, H. Yu, L. Yang, R. Liao and Z. L. Wang, *ACS Nano* **2018**, *12*, 3954-3963.

[8] Z. Zhao, Z. Zhang, L. Xu, F. Gao, B. Zhao, Z. Kang, Q. Liao and Y. Zhang, *Nano Energy* **2020**, *76*.

[9] Y. Liu, Y. Ji and Y. Yang, *Nanomaterials (Basel)* **2021**, *11*.

[10] K. Zhao, W. Sun, X. Zhang, J. Meng, M. Zhong, L. Qiang, M.J. Liu, B.N. Gu, C.C. Chung, M. Liu, F. Yu and Y.L. Chueh, *Nano Energy* **2022**, *91*.

[11] C. Chen, S. Zhao, C. Pan, Y. Zi, F. Wang, C. Yang and Z. L. Wang, *Nat. Commun.* **2022**, *13*, 1391.

[12] Q. Xu, J. Wen and Y. Qin, *Nano Energy* **2021**, *86*.

[13] S. Wang, Z. L. Wang and Y. Yang, *Adv. Mater.* **2016**, *28*, 2881-2887.

[14] J. Qi, N. Ma and Y. Yang, *Adv. Mater. Interfaces* **2018**, *5*.

[15] X. Chen, X. Ma, W. Ren, L. Gao, S. Lu, D. Tong, F. Wang, Y. Chen, Y. Huang, H. He, B. Tang, J. Zhang, X. Zhang, X. Mu and Y. Yang, *Cell Rep. Phys. Sci.* **2020**, *1*.

[16] S. Wang, X. Mu, X. Wang, A. Y. Gu, Z. L. Wang and Y. Yang, *ACS Nano* **2015**, *9*, 9554-9563.

[17] Y. Ji, K. Zhang and Y. Yang, *Adv. Sci. (Weinh)* **2018**, *5*, 1700622.

[18] K. Zhao, B. Ouyang, C. R. Bowen, Z. L. Wang and Y. Yang, *Nano Energy* **2020**, *71*.

[19] X. Fan, J. He, J. Mu, J. Qian, N. Zhang, C. Yang, X. Hou, W. Geng, X. Wang and X. Chou, *Nano Energy* **2020**, *68*.

[20] Q. Zhang, L. Li, T. Wang, Y. Jiang, Y. Tian, T. Jin, T. Yue and C. Lee, *Nano Energy* **2021**, *90*.

[21] N. Ma, K. Zhang and Y. Yang, *Adv. Mater.* **2017**, *29*.

[22] A. Sultana, M. M. Alam, T. R. Middya and D. Mandal, *Appl. Energy* **2018**, *221*, 299-307.

[23] J. He, T. Wen, S. Qian, Z. Zhang, Z. Tian, J. Zhu, J. Mu, X. Hou, W. Geng, J. Cho, J. Han, X. Chou, C. Xue, *Nano Energy* **2018**, *43*, 326-339.

[24] A. A. Khan, R. Saritas, M. M. Rana, N. Tanguy, W. Zhu, N. Mei, S. Kokilathasan, S. Rassel, Z. Leonenko, N. Yan, E. Abdel-Rahman, and D. Ban, *ACS Appl. Mater. Interfaces* **2022**, *14*, 4119-4131.

[25] K. Zhang, S. Wang and Y. Yang, *Adv. Energy Mater.* **2016**, *7*.

[26] B. Li, H. Liu, Y. Sun, Y. Cao and Y. Guo, *J. Mater. Sci. Mater. El.* **2022**, *33*, 5335-5340.

[27] T. Y. Kim, S. K. Kim and S. W. Kim, *Nano Converg.* **2018**, *5*, 30.

[28] L. Su, H. Wang, Z. Tian, H. Wang, Q. Cheng and W. Yu, *Adv. Sci. (Weinh)* **2019**, *6*, 1901980.

[29] Y. Ji, K. Zhang, Z. L. Wang and Y. Yang, *Energy Environ Sci.* **2019**, *12*, 1231-1240.

[30] X. Zhou, G. Xue, H. Luo, C. R. Bowen and D. Zhang, *Prog. Mater. Sci.* **2021**, *122*.

[31] S. H. Ji, W. Lee and J. S. Yun, *J. Eur. Ceram. Soc.* **2022**, *42*, 1414-1424.

[32] S. Cui, J. Wang, L. Mi, K. Chen, W. Ai, L. Zhai, X. Guan, Y. Zheng and D. Wang, *Nano Energy* **2022**, *91*.

[33] Y. Guo, Y. Chen, J. Ma, H. Zhu, X. Cao, N. Wang and Z. L. Wang, *Nano Energy* **2019**, *60*, 641-648.

[34] T. Zhao, W. Jiang, D. Niu, H. Liu, B. Chen, Y. Shi, L. Yin and B. Lu, *Appl. Energy* **2017**, *195*, 754-760.

FIGURE CAPTIONS

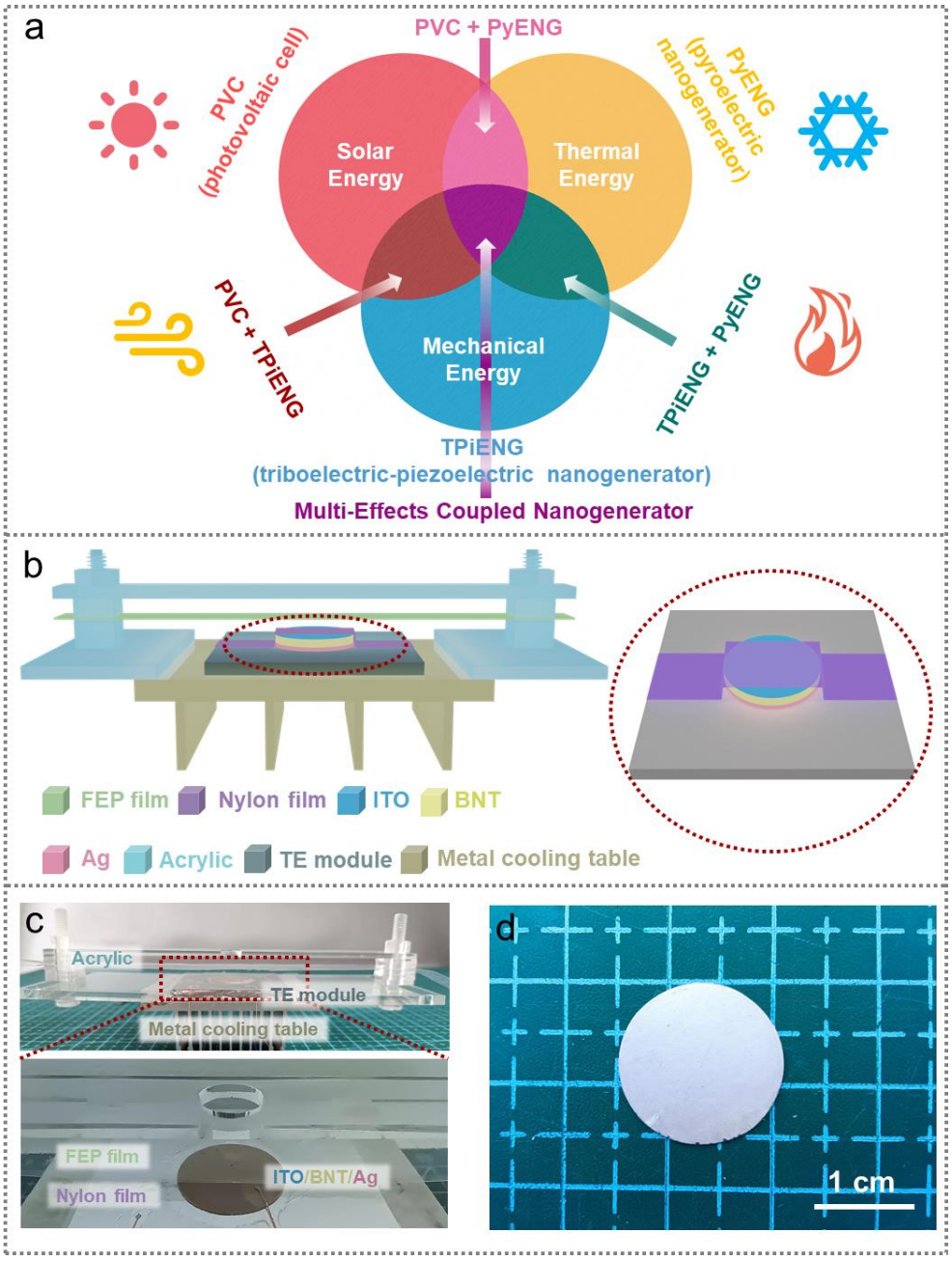

Figure 1. Structural design of coupled nanogenerator with multiple input effects. a) Design principle of the coupled nanogenerator. b) Schematic of the structure of the coupled nanogenerator, with a partial enlargement on the right; TE is a thermoelectric module. c) Physical view of the coupled nanogenerator device with partial enlargement below. d) Photo of ferroelectric BNT ceramics with 1 cm scale.

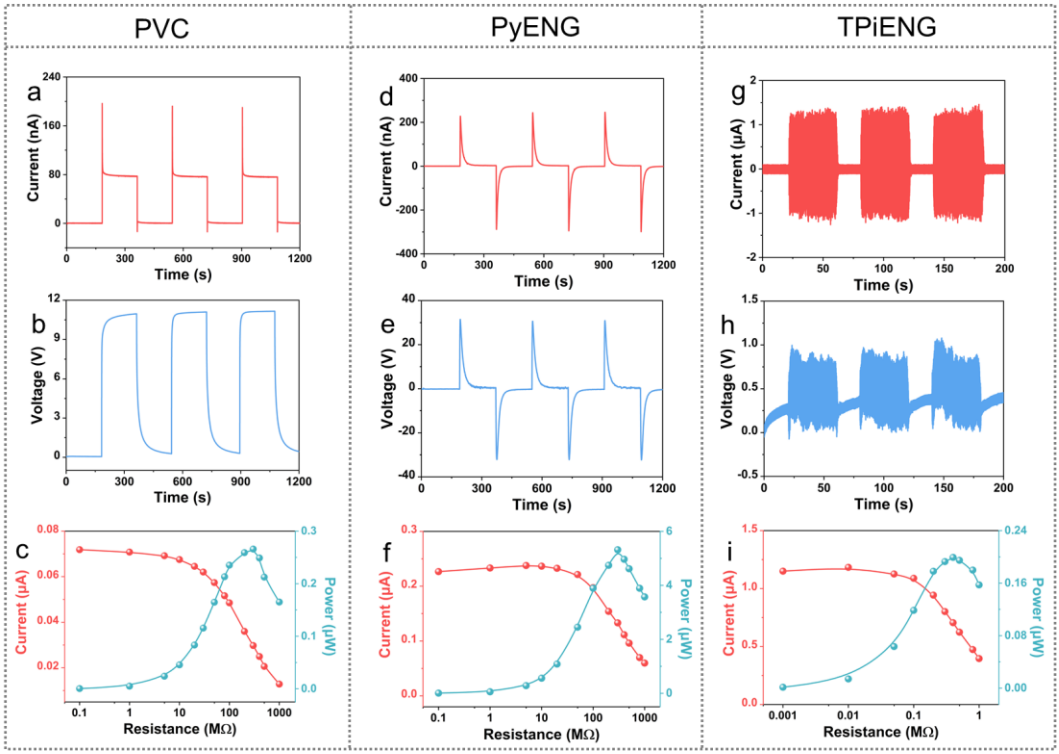

Figure 2. Output of single PVC, PyENG and TPiENG. a) Current signals, b) voltage signals, c) current at applied resistance and corresponding instantaneous power of PVC. d) Current signals, e) voltage signals, f) current at applied resistance and corresponding instantaneous power of PyENG. g) Current signals, h) output voltage signals, i) current at applied resistance and corresponding instantaneous power of TPiENG.

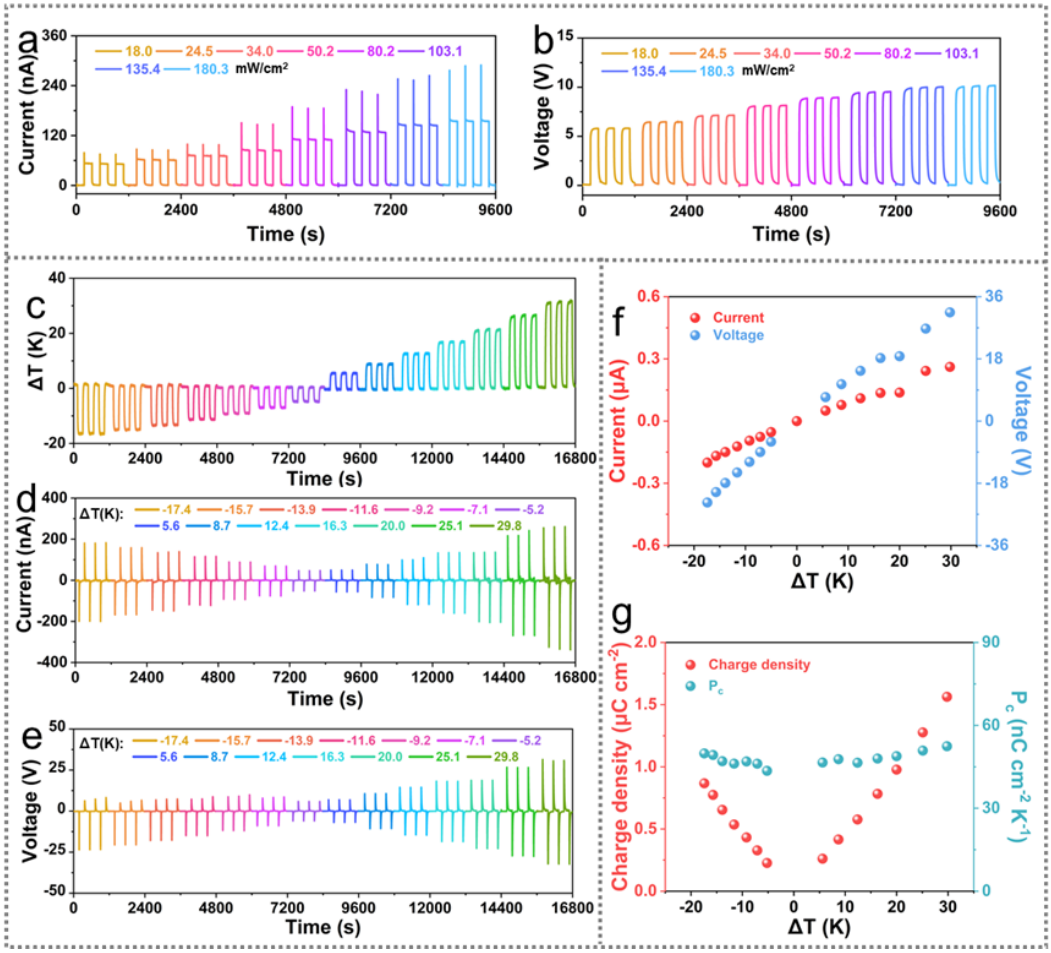

Figure 3. Output of individual PVC and PyENG at changing conditions. a) Current signals and b) voltage signals of PVC at different light intensities. c) Under changing temperature, d) the current and e) voltage of the PyENG corresponding to periodic temperature conditions. f) Current and voltage of the PyENG versus temperature difference. g) Charge density and pyroelectric coefficient calculated from the current for different temperature differences.

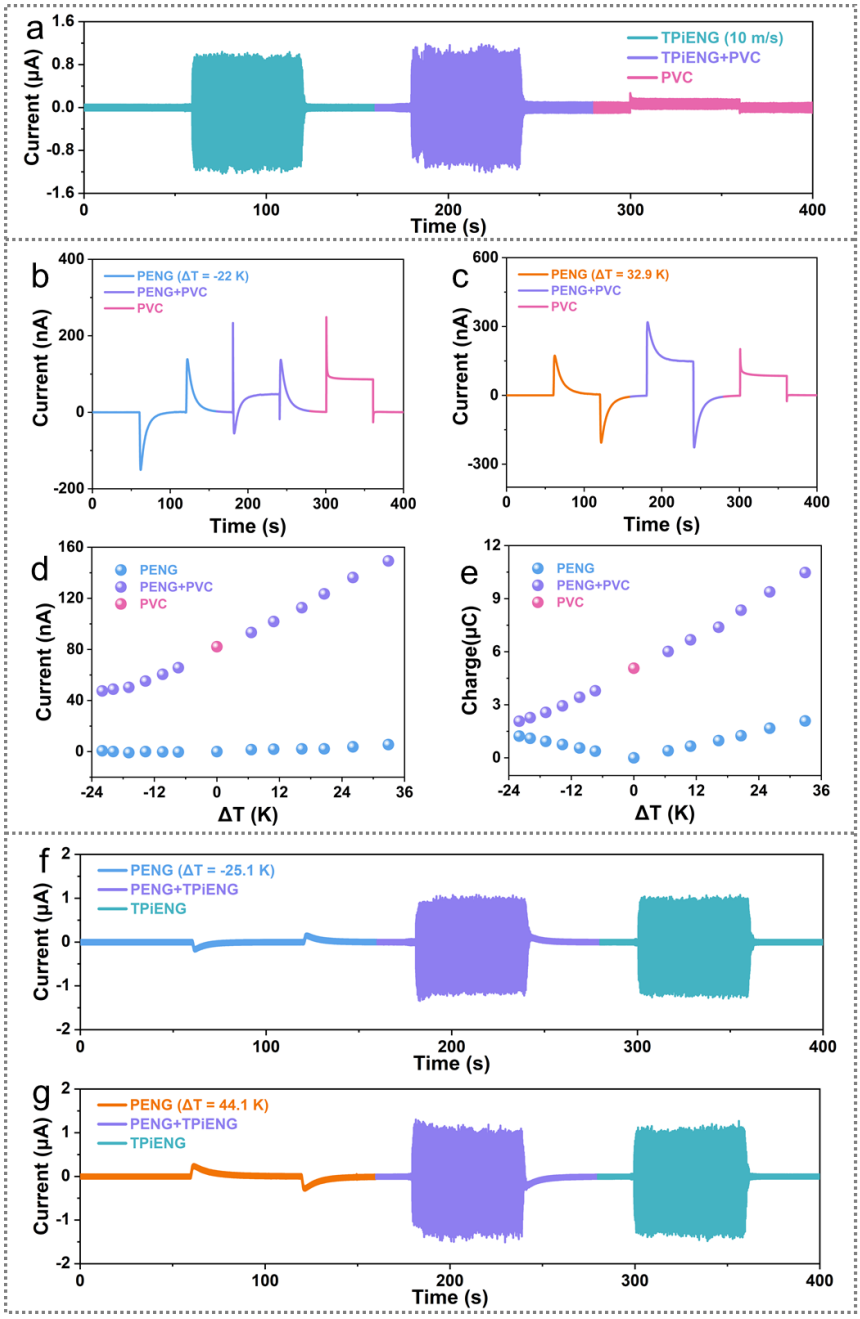

Figure 4. Coupling effects between any two of PVC, PyENG and TPiENG devices. a) Current signals curves between PVC and TPiENG after coupling and when operating independently. Current signals curves between PVC and PyENG after coupling under b) cooling conditions and c) heating conditions and when operating independently. d) Platform current and e) transferred charge at different temperature differences after coupling between PVC and PyENG and when operating independently. Current signals curves of PyENG and TPiENG under f) cooling conditions and after coupling under g) heating conditions versus when operating independently.

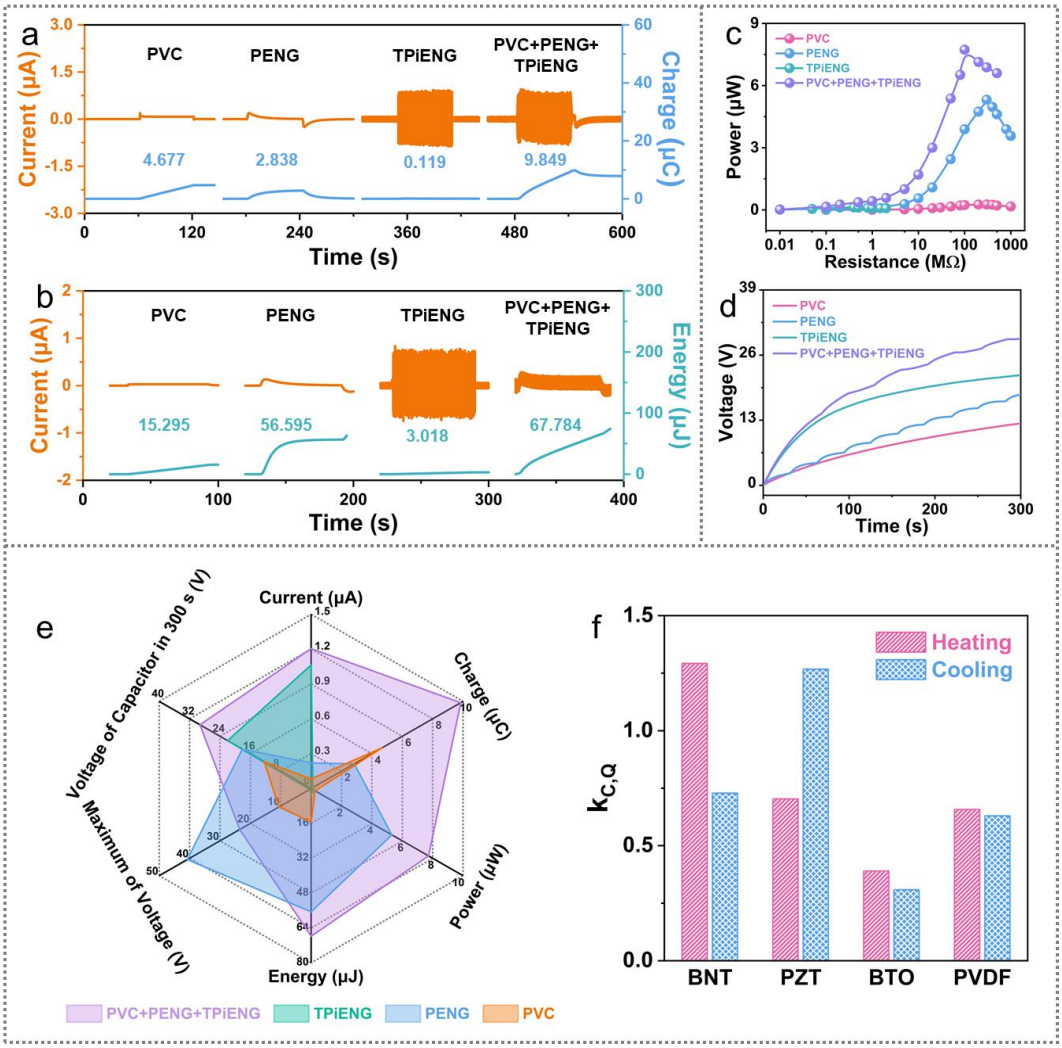

Figure 5. Output of coupled nanogenerators when multiple effects are acting simultaneously. a) Output currents and corresponding transferred charge with time. b) Current and energy with time corresponding to the power at maximum. c) Power when impedance matched with different resistances. d) Voltage signals profile across the capacitor when charging a 1 μF capacitor. e) Radar plot of output after coupling, compared to when operating independently. f) Comparison graph of coupling factor for different ferroelectric materials.